ORGANISMAL BIOLOGY

A carnivorous mushroom paralyzes and kills nematodes via a volatile ketone

Ching-Han Lee[1]†, Yi-Yun Lee[1,2]†, Yu-Chu Chang[3], Wen-Li Pon[1], Sue-Ping Lee[1], Niaz Wali[4,5,6], Takehito Nakazawa[7], Yoichi Honda[7], Jiun-Jie Shie[4,5,6], Yen-Ping Hsueh[1,2,8,9,10]*

The carnivorous mushroom *Pleurotus ostreatus* uses an unknown toxin to rapidly paralyze and kill nematode prey upon contact. We report that small lollipop-shaped structures (toxocysts) on fungal hyphae are nematicidal and that a volatile ketone, 3-octanone, is detected in these fragile toxocysts. Treatment of *Caenorhabditis elegans* with 3-octanone recapitulates the rapid paralysis, calcium influx, and neuronal cell death arising from fungal contact. Moreover, 3-octanone disrupts cell membrane integrity, resulting in extracellular calcium influx into cytosol and mitochondria, propagating cell death throughout the entire organism. Last, we demonstrate that structurally related compounds are also biotoxic to *C. elegans*, with the length of the ketone carbon chain being crucial. Our work reveals that the oyster mushroom has evolved a specialized structure containing a volatile ketone to disrupt the cell membrane integrity of its prey, leading to rapid cell and organismal death in nematodes.

INTRODUCTION

Chemical warfare is a common feature of predator-prey interactions. Predators such as snakes and spiders adopt modified fangs or radulae to release venom that targets prey. These neurotoxic venoms primarily affect the peripheral nervous system, in particular, neuromuscular junctions, to paralyze prey, although some elapid snake venoms also induce muscle necrosis mediated by enzymatically dependent plasma membrane damage (*1*–*3*). Some prey species have evolved specialized structures, such as the fin spines of fish or the glandular trichomes of plants, to store venom and secondary metabolites that are used to defend themselves from predation (*4*–*6*).

In the fungal kingdom, carnivorous fungi display diverse chemical strategies to target their prey, i.e., nematodes, the most abundant animals in soil (*7*–*9*). Among these nematophagous fungi, nematode-trapping fungi of the Ascomycota and the oyster mushroom of the Basidiomycota are the best-known examples. The nematode-trapping fungi produce several volatile compounds that mimic nematode food and sex cues to lure their nematode prey, eavesdropping on nematode ascaroside pheromones, and they develop various nematode-trapping devices such as adhesive networks, adhesive knobs, and constricting rings to capture the prey (*10*–*13*). In contrast, the oyster mushroom, *Pleurotus ostreatus*, has evolved a distinct strategy. Instead of physically snaring the nematode prey, its hyphae produce potent toxins that paralyze nematodes within a few minutes of contact (*14*). These toxins elicit massive calcium influx and systematic cell necrosis throughout the neuromuscular system of the nematodes via their externally exposed sensory cilia (*15*). A previous study reported that trans-2-decenedioic acid purified from *P. ostreatus* exhibited nematocidal activity (*16*), but this compound did not recapitulate the fast-acting paralysis and cell necrosis triggered by *P. ostreatus* hyphae (*15*), indicating that the key nematocidal compound produced by *P. ostreatus* remained to be identified. Moreover, the molecular mechanism by which systemic cell death is triggered in *Caenorhabditis elegans* is also uncertain.

Naturally produced toxins that can kill nematodes have frequently been isolated from microbes that occupy the same ecological niche as nematodes. The most widely used antiparasitic drug in human and veterinary medicine, ivermectin, is derived from avermectins purified from *Streptomyces avermitilis*, which activates glutamate-gated chloride channels in the nervous system to induce persistent paralysis (*17*–*19*). Another bacterially derived nematicide is the crystal proteins produced by *Bacillus thuringiensis*. Once ingested by a nematode, crystal proteins are proteolytically activated in the intestine and bind to membrane receptors, leading to pore formation and triggering the necrosis pathway mediated by aspartic protease (*20*, *21*).

In this study, we show through genetic screens that *P. ostreatus* relies on a specialized structure, toxocysts, to paralyze the nematode *C. elegans*. A volatile compound, 3-octanone, stored inside toxocysts is a major component triggering rapid paralysis and cell death in this nematode prey. Using in vivo and in vitro approaches, we demonstrate that 3-octanone disrupts cell membrane integrity in multiple *C. elegans* tissues, including sensory neurons, muscle cells, and hypodermis, causing massive calcium influx into the mitochondria and leading to cell death. Furthermore, we observed progressive adenosine 5′-triphosphate (ATP) depletion and a wave of mitochondrial calcium influx in the hypodermis that contributed to the propagation of cell death throughout the entire organism.

[1]Institute of Molecular Biology, Academia Sinica, Taipei 11529, Taiwan. [2]Molecular Cell Biology, Taiwan International Graduate Program, Academia Sinica and Graduate Institute of Life Science, National Defense Medical Center, Taipei, Taiwan. [3]Department of Biochemistry and Molecular Cell Biology, School of Medicine, Taipei Medical University, Taipei 11031, Taiwan. [4]Institute of Chemistry, Academia Sinica, Taipei 11529, Taiwan. [5]Institute of Biochemical Sciences, National Taiwan University, Taipei 10617, Taiwan. [6]Chemical Biology and Molecular Biophysics, Taiwan International Graduate Program, Academia Sinica, Taipei 10617, Taiwan. [7]Graduate School of Agriculture, Kyoto University, Sakyo-ku, Kyoto 606-8502, Japan. [8]Department of Biochemical Science and Technology, National Taiwan University, Taipei 10617, Taiwan. [9]Institute of Biochemistry and Molecular Biology, College of Medicine, National Taiwan University, Taipei 10051, Taiwan. [10]Department of Biochemical Science and Technology, National Chiayi University, Chiayi City 60004, Taiwan.
†These authors contributed equally to this work.
*Corresponding author. Email: pinghsueh@gate.sinica.edu.tw

This calcium wave is a dosage-dependent response that can be affected by muscle contraction and cell membrane fluidity. Last, we show that compounds structurally related to 3-octanone can also induce nematode paralysis and cell necrosis and that the length of the carbon chain is critical for nematocidal toxicity. Our work reveals that natural metabolites may gain an additional biological function via morphological evolution of the cell.

RESULTS

Toxocysts on *P. ostreatus* hyphae are essential for paralyzing *C. elegans*

To gain insights into the mechanism by which the oyster mushroom paralyzes its nematode prey, we conducted random ultraviolet (UV) and ethyl methansulfonate (EMS) mutagenesis on wild-type *P. ostreatus* using protoplasts generated from monokaryotic hyphae and then screened for mutants that could not paralyze *C. elegans*. Overall, we screened ~12,000 random mutagenized clones, and we isolated 13 mutants displaying almost complete loss of toxicity (*lot*) to *C. elegans* (fig. S1 and movie S1). Upon examining the morphology of these mutants, it was clear that the hyphae of nontoxic mutants all lacked numerous spherical structures prominent on wild-type hyphae (Fig. 1, A and B, and fig. S1B), which were similar to what have been described previously as toxocysts in other *Pleurotus* species (*22*), demonstrating that these toxocysts are essential for *P. ostreatus* to paralyze *C. elegans*. We observed that when *C. elegans* contacted toxocyts on wild-type fungal hyphae, most of the animals exhibited immediate aversive behavior and retreated (Fig. 1D and movie S2). The toxocysts are fragile, rupturing immediately upon contact by nematodes. To provide independent evidence supporting that toxocysts are required to paralyze *C. elegans*, we added glass beads onto the agar surface where wild-type *P. ostreatus* hyphae were growing and shook them for a few seconds to disrupt the toxocysts. After shaking, we placed *C. elegans* immediately onto the *P. ostreatus* culture and observed their locomotion. In contrast to the almost instantaneous paralysis response upon contacting intact toxocysts, we observed that disrupting the toxocysts with glass beads enabled *C. elegans* to move freely on the fungal culture (Fig. 1C and movie S3), demonstrating that intact toxocysts are essential to nematode paralysis. Moreover, this instantaneous loss of toxicity upon glass bead treatment implied that the nematocidal toxin could be volatile in nature.

Gas chromatography–mass spectrometry analyses identify 3-octanone from glass bead–treated *P. ostreatus* culture

To test our hypothesis that the toxocysts contain a volatile nematicidal toxin, we conducted gas chromatography–mass spectrometry (GC-MS) using solid-phase microextraction under three different conditions. Under the first condition, the vial only contained the culture medium and glass beads. Under the second condition, the vial contained *P. ostreatus* that had been cultured for 2 to 3 weeks. Under the third condition, the vial contained *P. ostreatus* cultured for 2 to 3 weeks, as well as some glass beads that had been shaken vigorously just before sampling with the solid-phase microextraction (SPME) probe. The GC-MS profiles of these three conditions were analyzed and compared (Fig. 2A), resulting in the identification of 13 major compounds based on the total ion chromatogram (TIC). Notably, a single compound, compound **6**, was specifically detected under the condition of toxocyst disruption (Fig. 2A). GC-MS spectra and library searching revealed the chemical identity of compound **6** to be 3-octanone (fig. S2A). To confirm that volatile 3-octanone occurs in toxocysts, we treated wild-type and *lot* mutant cultures with hydroxylamine and subjected the samples to solid-phase extraction. When hydroxylamine reacts with 3-octanone, an oxime bond forms, resulting in the corresponding 3-octanone oxime (Fig. 2B). Therefore, we analyzed hydroxylamine-treated wild-type and six *lot* mutants (*lot1*, *lot2*, *lot5*, *lot6*, *lot9*, and *lot10*) by MS. We detected the presence of protonated ions of 3-octanone oxime at expected mass-to-charge ratio (m/z) values of 144.1 in the wild-type sample, but not in the *lot* mutants (Fig. 2B and fig. S2B). Thus, 3-octanone is likely a key compound stored in the toxocysts of *P. ostreatus*.

3-Octanone triggers paralysis, calcium influx, and cell necrosis in *C. elegans*

Next, we assessed whether 3-octanone exhibits bioactivity in *C. elegans*. To do so, we directly applied a gradient of 3-octanone concentrations to freely moving *C. elegans* to mimic contact with toxocysts on the fungal hyphae. We observed that this 3-octanone treatment paralyzed *C. elegans* at concentrations of >50% (Fig. 3A). In addition, it also paralyzed three additional free-living soil nematodes, *Rhabditis rainai*, *Oscheius mtriophila*, and *Pelodera teres* (fig. S3A), suggesting that 3-octanone exerts broad toxicity on diverse nematode species. Moreover, when we monitored calcium levels in the pharyngeal muscle cells of nematodes via the calcium indicator GCaMP6 (under the *myo-2* promoter) in response to 3-octanone contact, we found that they massively increased ($\Delta F/F_0 > 10$) in the pharyngeal corpus region (movie S4), mimicking the phenotype displayed by *C. elegans* upon contact with *P. ostreatus* toxocysts (Fig. 3B). In contrast, our solvent control (mineral oil) or *P. ostreatus lot* mutants did not elicit any increase in calcium levels in the pharynx of prey, demonstrating that the prominent calcium influx we observed was attributable to toxocysts and 3-octanone (Fig. 3B and fig. S3B).

We also assessed whether 3-octanone triggers cell necrosis in the ciliated sensory neurons of nematodes, representing another prominent feature observed when *C. elegans* contacted *P. ostreatus* (*15*). We applied 3-octanone to the *C. elegans* ciliated sensory neuron reporter line (P*osm-6*::GFP) and imaged the nematodes after 5 min. As shown in Fig. 3C, we observed obvious fragmentation of the neuronal processes and clearly swollen cell bodies of ciliated sensory neurons, again resembling the phenotypes of nematodes that contacted *P. ostreatus*. Together, these results demonstrate that 3-octanone triggers paralysis, calcium influx, and cell death in *C. elegans*, recapitulating the key phenotypes that we described previously as being triggered by *P. ostreatus* (*15*). Thus, 3-octanone likely represents a key nematocidal compound inside *P. ostreatus* toxocysts.

P. ostreatus triggers calcium influx in the mitochondrial matrix of paralyzed nematodes

To further characterize subcellular features of the rapid cell death triggered by *P. ostreatus* in multiple *C. elegans* tissues, we conducted transmission electron microscopy (TEM) on cross sections of the pharyngeal corpus in animals exposed to *P. ostreatus* or 3-octanone for 5 min. We observed marked mitochondrial enlargement in both pharyngeal and body wall muscle cells under both conditions (Fig. 4A). To assess whether the mitochondrial enlargement triggered by *P. ostreatus* and 3-octanone may occur in different

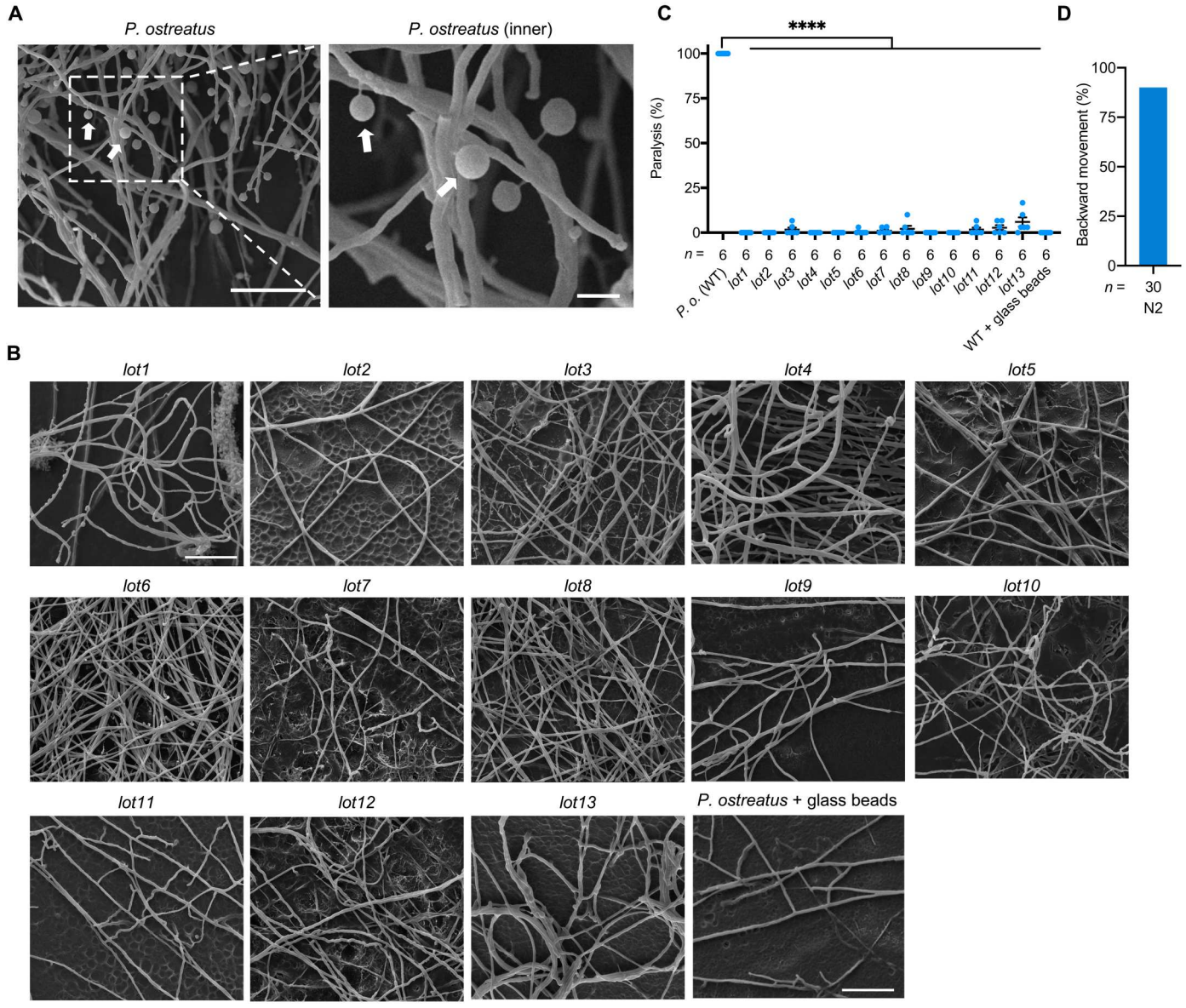

Fig. 1. *P. ostreatus* mutants lacking toxocyst structures are nontoxic to *C. elegans*. (**A** and **B**) Scanning electron microscopy (SEM) imaging of wild-type *P. ostreatus* (*P. o.*) (A), and *lot* mutant lines and a wild-type culture disrupted with glass beads (B). Arrows indicate the toxocysts. Scale bars, 50 and 10 μm (indicated region). (**C**) Paralysis ratio of adult N2 *C. elegans* in response to wild-type (WT) *P. ostreatus*, mutant lines, or wild-type *P. ostreatus* disrupted with glass beads (WT + glass beads). Each dot represents 30 or 15 animals (means ± SD; *n* is shown below the *x* axis). (****$P < 0.0001$). (**D**) Quantification of backward movement and paralysis in adult N2 contacting a *P. ostreatus* toxocyst.

tissues, we monitored the morphology of mitochondria by targeting green fluorescent protein (GFP) or GCaMP proteins to the mitochondrial matrix via the cytochrome *c* oxidase subunit 8 (COX8) mitochondrial signal sequence under the control of various promoters. We found that mitochondria changed from tubular to spherical in pharyngeal and body wall muscle cells upon *P. ostreatus* or 3-octanone contact (fig. S4, A and B), which is consistent with our TEM images. In ciliated sensory neurons and hypodermis, the mitochondria became punctate and fragmented upon exposure to *P. ostreatus* and 3-octanone (Fig. 4, B and C). Thus, contact with *P. ostreatus* and 3-octanone can rapidly alter mitochondrial morphology in *C. elegans*.

Mitochondrial morphology is regulated by ion homeostasis in the mitochondrial matrix, with calcium and potassium influxes playing crucial roles in enhancing osmotic pressure and water accumulation in the matrix (*23*). Our previous study showed that *P. ostreatus* triggers massive calcium influx in muscular and neuronal cytosols (*15*). To test whether excessive cytosolic calcium induces mitochondrial calcium uptake, we assessed mitochondrial calcium levels in pharyngeal and body wall muscle cells by targeting the calcium indicator GCaMP5 in the mitochondrial matrix. We observed an enhanced fluorescence signal (reflecting calcium levels) in the pharyngeal corpus and head muscles upon nematodes exposing to *P. ostreatus* hyphae (Fig. 4D and movie S5). This rapid

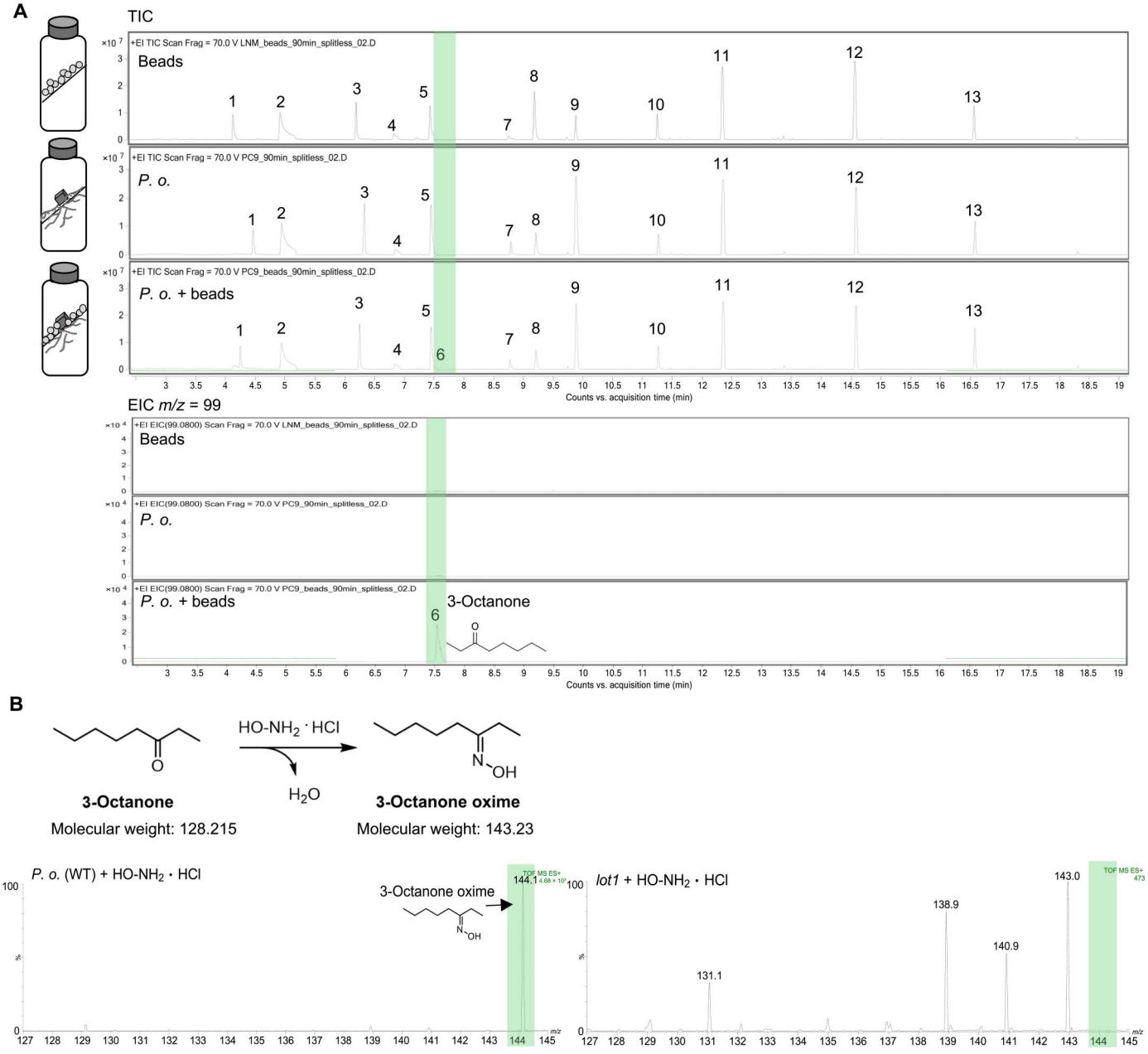

Fig. 2. GC-MS analysis reveals 3-octanone as a major compound inside toxocysts. (**A**) TIC and extracted ion chromatogram (EIC) of medium and glass bead control, medium inoculated with *P. ostreatus*, and medium inoculated with *P. ostreatus* and glass beads. Numbers 1 to 13 represent different compounds: (1) dimethylsilanediol, (2) hexamethylcyclotrisiloxane, (3) methoxy-phenyl-oxime; (4) 4-nitrophthalamide; (5) octamethylcyclotetrasiloxane; (6) 3-octanone; (7) hexamethylcyclotrisiloxane; (8) 2,5-bis[(trimethylsilyl)oxy]-benzaldehyde; (9) decamethylcyclopentasiloxane; (10) 4,6′-dimethoxy-2′-(*tert*-butyldimethylsilyl)oxychalcone; (11) dodecamethyl cyclohexasiloxane; (12) tetradecamethylcycloheptasiloxane; and (13) hexadecamethylcyclooctasiloxane. (**B**) Reaction of 3-octanone with HO-NH_2·HCl to generate 3-octanone oxime. The mass spectra of *P. ostreatus* wild-type (left) or *lot1* culture (right) treated with HO-NH_2·HCl are shown.

calcium uptake in mitochondria was not simply due to contact with fungal hyphae because the fluorescence signal did not increase upon contact with another nematode-trapping fungus *Arthrobotrys oligospora* or the *P. ostreatus lot1* mutant (Fig. 4D), indicating that direct contact with toxocysts is required to induce massive calcium influx in the pharynx.

Next, given the marked alteration in mitochondrial morphology that we observed in the hypodermis (Fig. 4C), we monitored mitochondrial calcium levels in that tissue after *C. elegans* contacted toxocysts. Unexpectedly, not only did we observe calcium uptake accompanying morphological changes in mitochondria but also a prominent calcium wave propagating throughout the hypodermis (Fig. 4, E and F, and movie S7). This calcium wave was initiated at the head of *C. elegans* and propagated at an average of ~50 μm/min through the hyp7 syncytium within 10 min, and the wave markedly slowed down after 10 to 15 min of exposure (Fig. 4G).

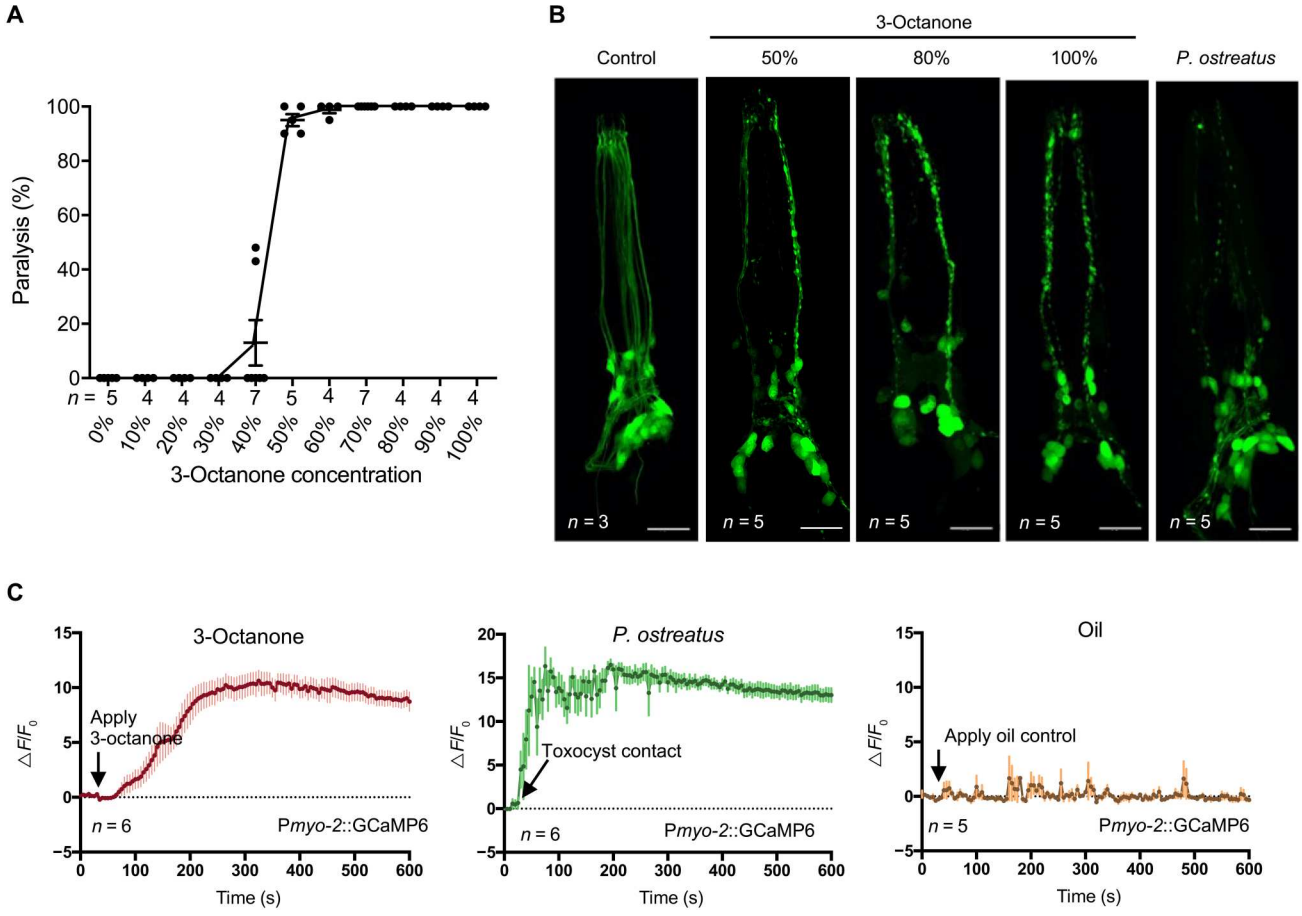

Fig. 3. 3-Octanone triggers paralysis and cell death in *C. elegans*. (**A**) Paralyzed ratio of adult N2 upon 3-octanone contact. Each dot represents 20 to 25 animals (means ± SEM; *n* is shown below the *x* axis). (**B**) GCaMP6 signals of the pharyngeal corpus of adult animals in response to 50% 3-octanone, *P. ostreatus*, or mineral oil as control (means ± SEM; *n* is shown above the *x* axis). (**C**) Fluorescence imaging of ciliated sensory neurons using cytosolic GFP reporter lines exposed to 3-octanone, *P. ostreatus*, or mineral oil for 5 min. Scale bars, 15 μm.

Soon after contacting toxocysts, mitochondrial GCaMP signals increased, and then the mitochondria adopted a spherical appearance (movie S7), implying that mitochondrial calcium uptake enhances osmolarity in the matrix, triggering water accumulation and causing mitochondrial enlargement and spherification. To examine whether propagation of the calcium wave in the hypodermis is dosage dependent, i.e., regulated by the number of toxocysts that a nematode contacts, we compared the distance a calcium wave traveled for individuals that touched a single toxocyst with that in individuals that touched multiple (~10) toxocysts. The calcium wave traveled on average of ~400 μm from the head after 10 min in *C. elegans* that touched multiple toxocysts (Fig. 4F). In contrast, for *C. elegans* that only touched a single toxocyst, the calcium wave only traveled ~100 μm from the head after 10 min, and it only traveled another ~50 μm after 1 hour (fig. S4, C and D), indicating that the calcium wave propagated much more slowly. These results imply that the mitochondrial calcium wave triggered by *P. ostreatus* is a dosage-dependent response.

P. ostreatus and 3-octanone disrupt nematode cell membrane integrity

How do toxocysts and 3-octanone trigger calcium influx in the cytosol and mitochondria of nematodes? We hypothesized that toxocysts and 3-octanone may disrupt cell membrane integrity, resulting in aberrant calcium influx into the cells. To test this hypothesis, we expressed myristoylated GFP (myrGFP) to label cell membranes and then examined their structure after the animals either contacted toxocysts or were exposed to 3-octanone. First, we monitored the plasma membranes of ciliated sensory neurons, representing the first point of contact with toxocysts and that are required for initiating the paralysis response in nematodes. We expressed myrGFP in intereukin-2 (IL-2) neurons under the *klp-6* promoter and observed that the neuronal processes became fragmented and truncated within a few minutes of exposure to either toxocysts or 3-octanone (Fig. 5A). Next, we monitored the plasma membranes of body wall muscle cells and observed that myrGFP signals along the plasma membrane, which were continuous in nontreated nematodes, became aggregated and fragmented in treated individuals (Fig. 5B). Furthermore, we used a membrane-bound GFP tag (memGFP) that contains the signal sequence and transmembrane domain of the PAT-3 protein (*24*) to visualize the plasma

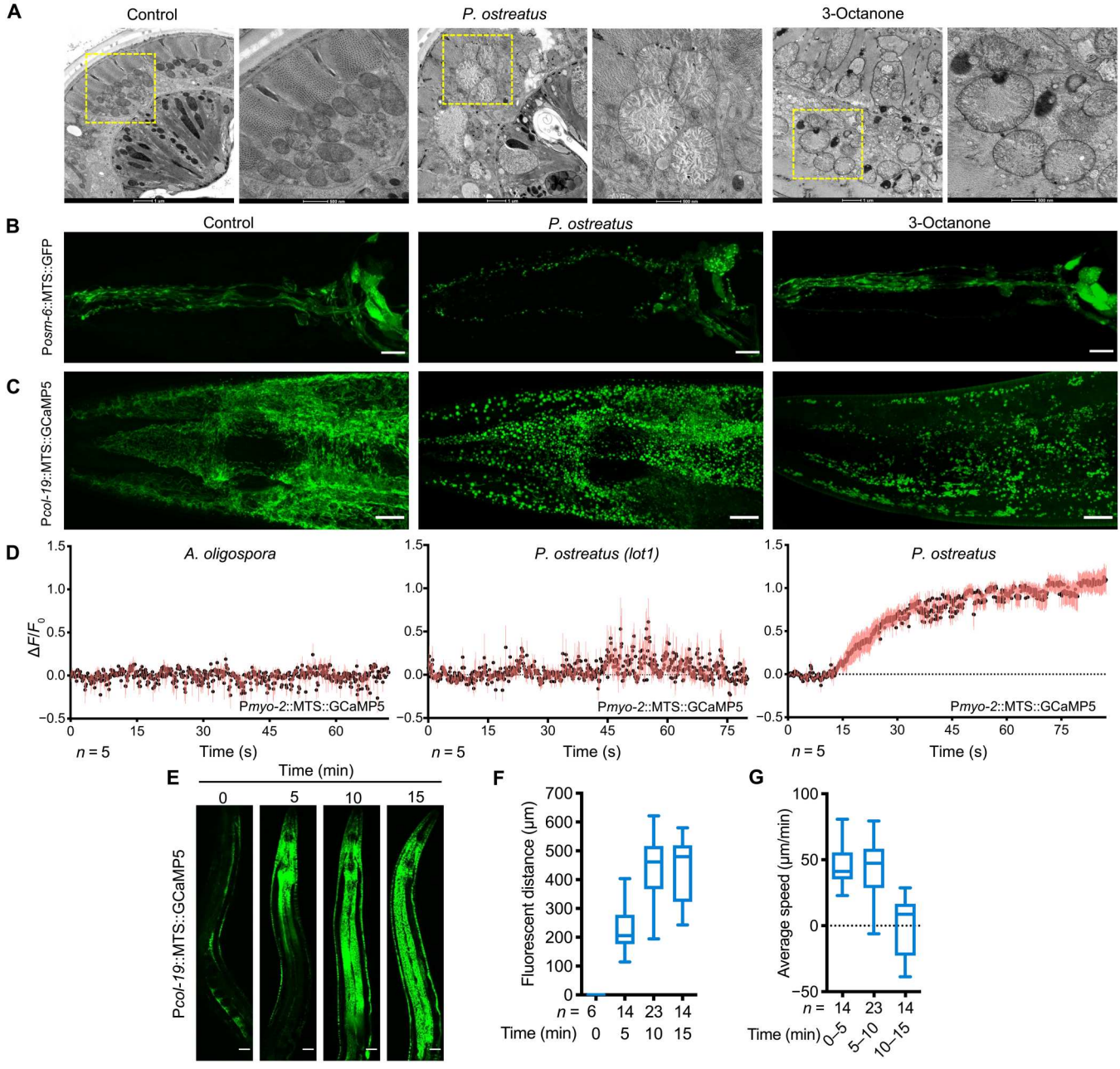

Fig. 4. *P. ostreatus* induces mitochondrial calcium influx and triggers a calcium wave in nematode hypodermis tissue. (**A**) TEM imaging of the head region of adult N2 exposed to *P. ostreatus* or 80% 3-octanone for 5 min. Control represents untreated nematodes. The indicated regions are magnified ×2.6 (right). Scale bars, 1 μm (left) and 500 nm (right). (**B** and **C**) Fluorescence imaging of mitochondria in ciliated sensory neurons (B) and hypodermis (C) using mitochondrial GFP or GCaMP5 reporter lines exposed to *P. ostreatus* or 80% 3-octanone for 5 min. Scale bars, 10 μm. (**D**) Mitochondrial GCaMP5 signals of the pharyngeal corpus of adult N2 in response to *P. ostreatus* or *A. oligospora* hyphae (means ± SEM; *n* is shown above the *x* axis). (**E**) Fluorescence imaging of hypodermis expressing mitochondrial GCaMP5 in nematodes that have been exposed to *P. ostreatus* over time. Scale bars, 25 μm. (**F**) Quantification of the extent of mitochondrial GCaMP5 fluorescent signal in the hypodermis. (**G**) Average speed of activated mitochondrial GCaMP5 fluorescent signal in the hypodermis upon fungal contact.

membrane of the hypodermis. Again, GFP signals became aberrantly aggregated soon after *P. ostreatus* or 3-octanone exposure (Fig. 5C). Accordingly, we speculate that 3-octanone rapidly disrupts the integrity of cell membranes in various *C. elegans* tissues.

Next, we extracted total lipids from *C. elegans* and used them to reconstitute liposomes in vitro to test whether 3-octanone affects their properties. First, we assayed liposome aggregation based on turbidity measurements. As shown in Fig. 5D, turbidity (absorbance of liposome samples at 400 nm) increased upon the addition of 3-octanone, indicating that it triggered liposome aggregation and fusion. In addition, we also used TEM to observe the morphology of liposomes in the absence or presence of 3-octanone, which revealed

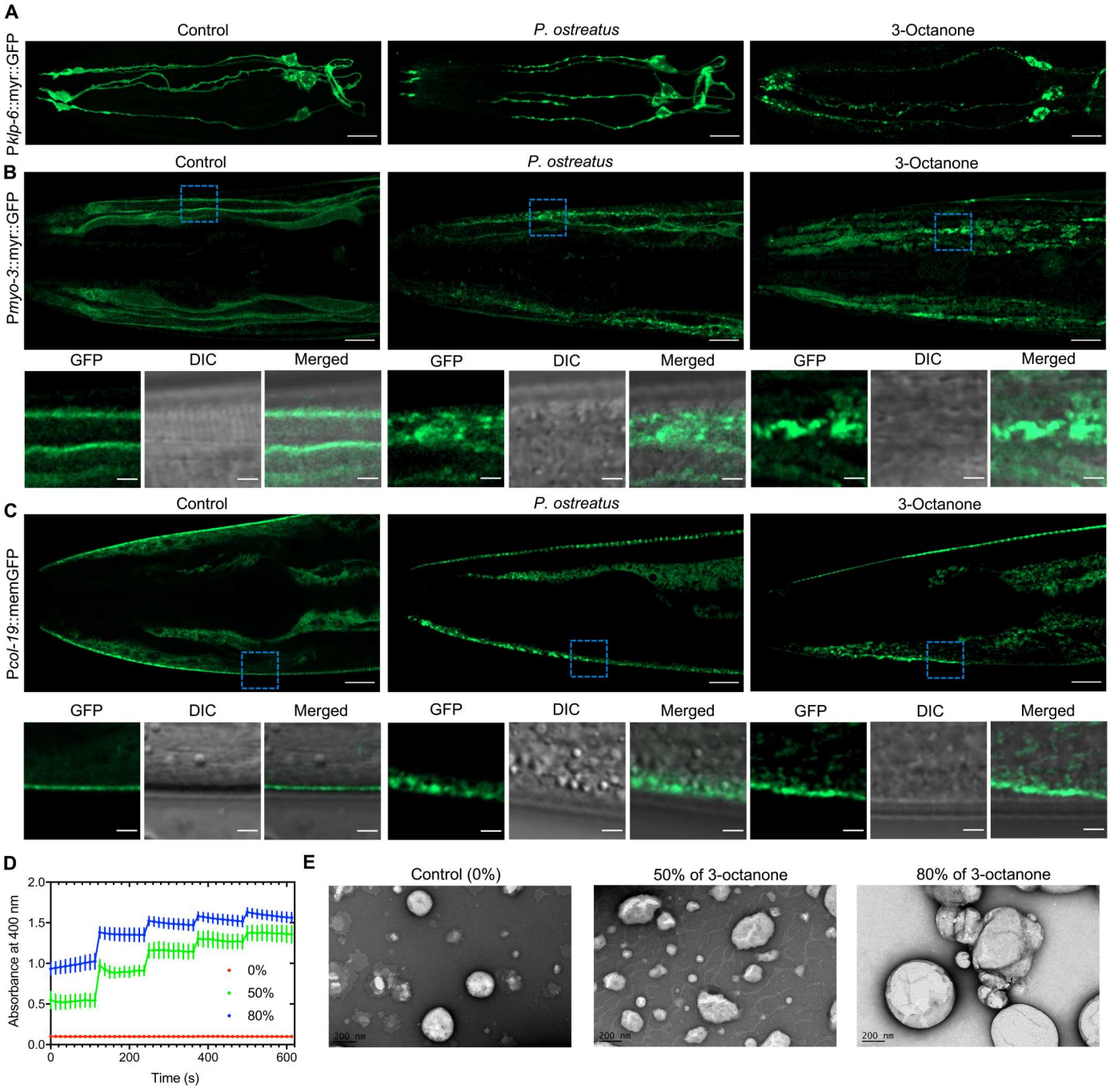

Fig. 5. *P. ostreatus* and 3-octanone impair plasma membrane integrity. (**A** to **C**) Fluorescence imaging of plasma membranes in body wall muscles (A), IL-2 neurons (B), and hypodermis (C) using myrGFP or memGFP reporter lines exposed to *P. ostreatus* or 80% 3-octanone for 10 min. The indicated regions are enlarged in the insets displaying GFP alone (left), differential interference contrast (DIC) alone (middle), or GFP and DIC overlays (right). Scale bars, 10 and 2 μm (inset). (**D**) Time course of turbidity measurements for liposomes prepared from *C. elegans* lipid extracts mixed with 50 or 80% 3-octanone. (**E**) TEM imaging of liposomes prepared from *C. elegans* lipid extracts (control) or those mixed with 50 or 80% 3-octanone. Scale bars, 200 nm.

that liposomes became larger and their surfaces were rougher than controls in the presence of 3-octanone (Fig. 5E). These findings demonstrate that 3-octanone alters liposomes of nematode lipids in vitro and, thus, that 3-octanone may disrupt membrane integrity, causing extracellular calcium influx into cells in vivo.

P. ostreatus and 3-octanone induce cell death throughout *C. elegans*

To validate that membrane disruption is associated with the rapid cell necrosis observed in neurons and muscle cells of *C. elegans* (*15*), we performed propidium iodide (PI) staining on paralyzed nematodes. PI cannot permeabilize into live cells due to the intact cell

membrane barrier, whereas nuclei of dead cells exhibit strong fluorescence. We observed that the nuclei of healthy animals did not present a fluorescence signal following 2 hours of PI treatment (Fig. 6A). However, upon exposure to *P. ostreatus*, cells with fluorescent nuclei were detected within 5 min, and the fluorescence signal progressively became stronger in nuclei along the anteroposterior body axis (Fig. 6A), showing that cell death propagated from the head of *C. elegans*. Similarly, we observed multiple PI-positive nuclei from the head to the body in nematodes treated with 3-octanone (Fig. 6A). Dauers also displayed PI-positive nuclei in the head upon treatment with *P. ostreatus* or 3-octanone (fig. S5), consistent with our previous study showing that all nematode stages are susceptible to *P. ostreatus*–elicited paralysis (*15*). This form of cell death is unlikely to represent a form of apoptosis because *ced-3* and *ced-4* mutants exhibit the same phenotype (fig. S5B).

Given that the calcium wave in the hypodermis was correlated with the number of toxocysts that nematodes had contacted, we tested whether the degree of cell death also correlated with the number of toxocysts touched by nematodes. We counted more dead cells in animals that had contacted multiple (~10) toxocysts than in those that had contacted a single one (Fig. 6B and fig. S5C), supporting that cell death propagation is also dosage dependent.

Necrotic cell death is triggered by ATP depletion (*25*). To test whether the propagated cell death triggered by *P. ostreatus* is accompanied by ATP depletion, we constructed transgenic nematodes hosting the ATP indicator QUEEN-2m (*26*), which we expressed in pharyngeal muscle cells and hypodermis using the *myo-2* and *col-19* promoters, respectively. This sensor comprises a circularly permuted enhanced GFP inserted in a bacterial ATP-binding protein, and its signal intensity is measured by peak emission at 525 nm and excitation wavelengths of 405 and 488 nm. We observed that upon exposing nematodes to *P. ostreatus* or 3-octanone for 10 min, the 405/488 excitation ratio in pharyngeal muscle was reduced to 0.5 or 0.6, respectively (Fig. 6, C and D), evidencing rapid ATP depletion in the pharynx of paralyzed nematodes. Moreover, ATP levels became progressively depleted in the hypodermis upon *P. ostreatus* and 3-octanone exposure, with the 405/488 excitation ratio being reduced in hyp4, hyp3, and hyp6 cells after 10 min of exposure and being reduced through hyp7 cells 30 min later (Fig. 6, E and F), indicating that ATP depletion also propagates in an anterior-to-posterior direction in *C. elegans*.

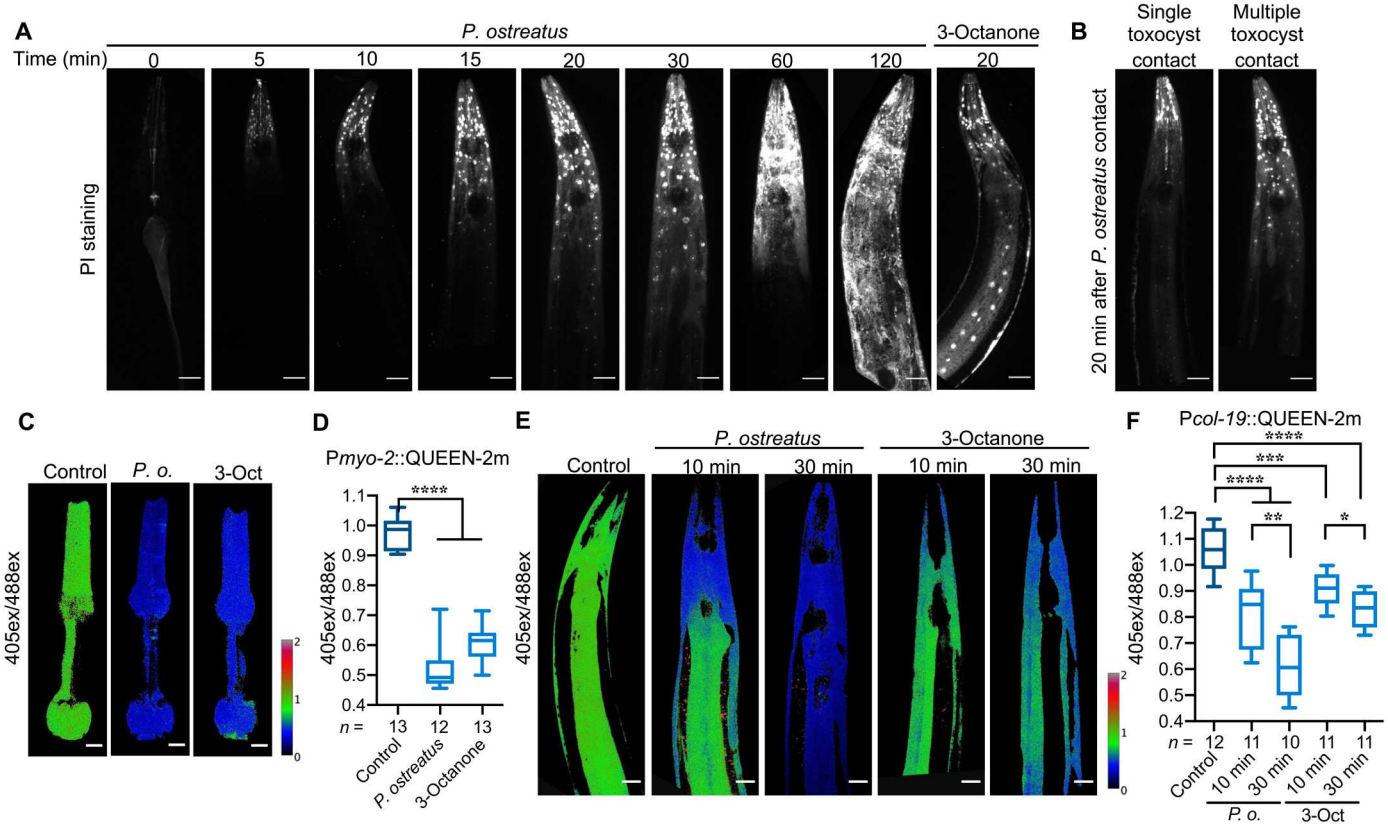

Fig. 6. *P. ostreatus* triggers organismal death. (**A**) Fluorescence imaging over time of PI staining in adult N2 exposed to *P. ostreatus* or 3-octanone for 20 min. The 0 time point represents healthy nematodes stained with PI solution for 2 hours. Scale bars, 25 μm. (**B**) Fluorescence imaging of PI staining in N2 after contact with single or multiple toxocysts for 20 min. Scale bars, 25 μm. (**C** to **F**) Relative ATP levels in pharyngeal muscles (C and D) and hypodermis (E and F) of N2 upon contact with *P. ostreatus* or 3-octanone (3-oct) for 10 or 30 min, as measured by the 405/488 excitation (405ex/488ex) ratio of the ATP sensor QUEEN-2m. Quantifications of the 405/488 excitation ratios ranging from 0 (blue) to 2 (red) in the pharynx and hypodermis are shown in (D) and (F), respectively. Scale bars, 10 μm. (*$P < 0.05$, **$P < 0.01$, ***$P < 0.001$, and ****$P < 0.0001$).

The hypodermis calcium wave and cell death can be regulated by cell membrane fluidity and muscle contraction

Our observation of rapid membrane rupture after nematodes contacted toxocysts and 3-octanone prompted us to consider if the lipid composition of the cell membrane mediates susceptibility to the *P. ostreatus* toxin. The PAQR -2IGLR-2 complex senses membrane rigidity to enhance unsaturated fatty acid production, and the *paqr-2* and *iglr-2* mutants exhibit impaired membrane homeostasis under cold conditions, whereby excess saturated fatty acids in their plasma membranes reduce membrane fluidity (*27*–*29*). We examined how these mutants responded to *P. ostreatus* and observed mitochondrial calcium uptake in their head hypodermis, but, notably, propagation of the calcium waves was substantially diminished, on average, progressing only ~100 μm from the head after 10 min and ~200 μm after 1 hour (Fig. 7, A and B, and fig. S6A). Upon contacting toxocysts, these mutants also presented much fewer PI-positive cells that were restricted to the anterior head region (Fig. 7C and fig. S6B). Moreover, we found that when *paqr-2* and *iglr-2* were grown on medium supplied with small amounts of detergents (0.01% IGEPAL) to increase membrane fluidity (*30*, *31*), the calcium wave and cell death propagation phenotypes were partially restored (Fig. 7, A to C). These results demonstrate that an excess of saturated fatty acids may slow down toxin diffusion and propagation of the calcium wave and cell death in *C. elegans*.

P. ostreatus triggers rapid calcium influx in muscle cells, leading to muscle hypercontraction. To explore whether muscle contraction accelerates toxin diffusion in *C. elegans*, we tested mutant nematode lines that are incapable of muscle contraction due to loss of structural components of the musculature, i.e., *unc-54* (myosin heavy chain) and *unc-60* (cofilin). The *unc-54* and *unc-60* mutants displayed extremely slow propagation of the calcium wave and diminished cell death upon forced contact with multiple toxocysts (Fig. 7, D to F). Furthermore, treatment of nematodes with ivermectin, which inhibits muscle contraction (*18*), also restricted propagation of both the calcium wave and consequent cell death (Fig. 7, D to F, and fig. S6, C and D). These results indicate that the mechanical force triggered by muscle contraction contributes to toxin diffusion, promoting calcium wave propagation and cell death throughout the nematode.

Ketone carbon number is crucial for biotoxicity

3-Octanone is a common volatile organic compound (VOC) that has been identified in diverse organisms, including fungi. To further examine which chemical properties of 3-octanone are crucial for nematode toxicity, we tested a gradient of 2-octanone

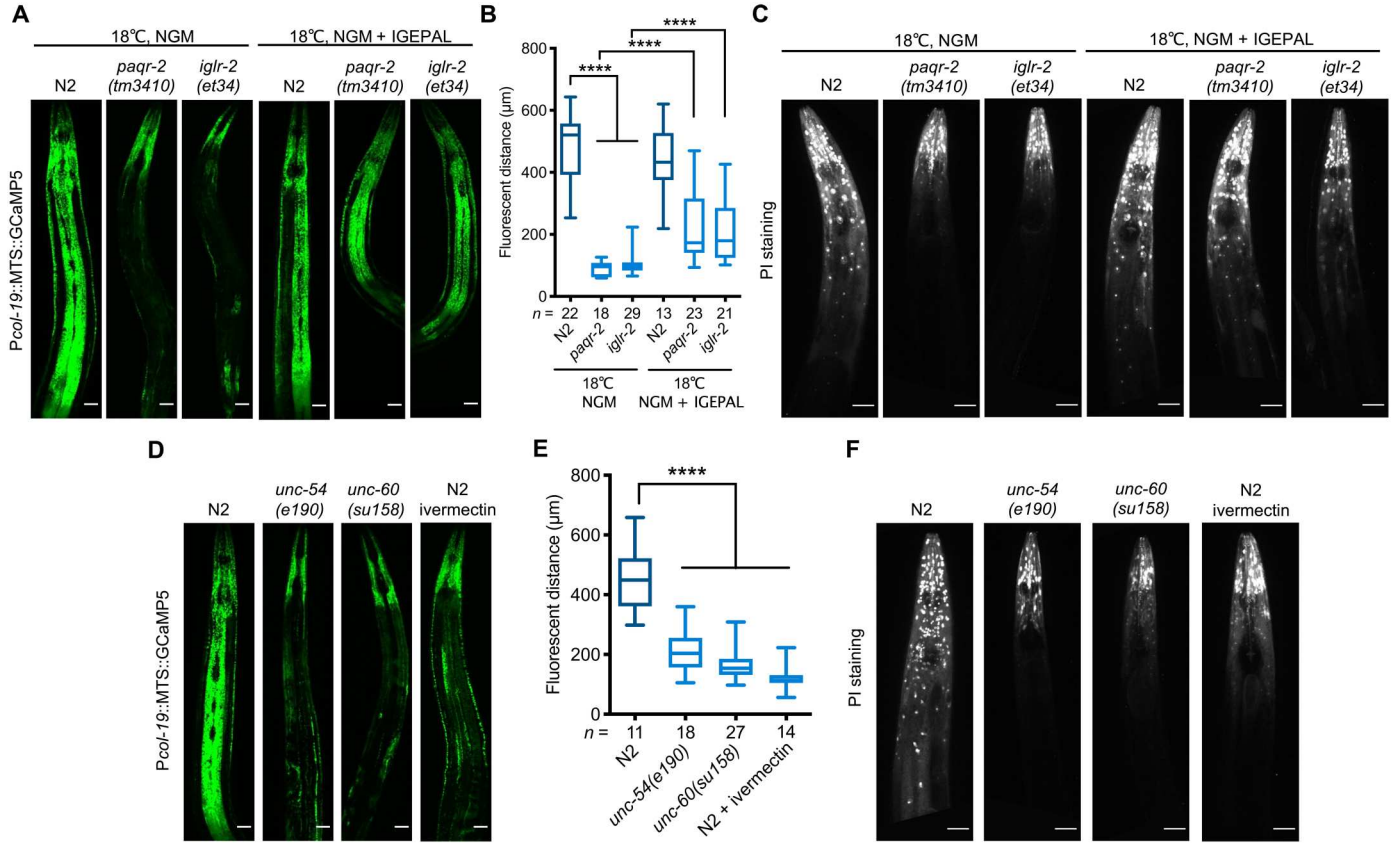

Fig. 7. Cell membrane fluidity and muscle contraction affect mitochondrial calcium-propagated waves and organismal death. (**A** and **D**) Fluorescence imaging of N2 hypodermis expressing mitochondrial GCaMP5 in nematodes after exposure to *P. ostreatus* for 10 min. The animals were grown at 18°C on nematode growth medium (NGM) or NGM and 0.01% IGEPAL plates (A and **B**). Adult N2 was treated with 10 μM ivermectin for 40 min and that then contacted multiple *P. ostreatus* toxocysts. (D and **E**) Quantifications of the extent of mitochondrial GCaMP5 fluorescence in the hypodermis are shown in (B) and (E). Scale bars, 25 μm. (**C** and **F**) Fluorescence imaging of PI-stained nematodes after exposure to *P. ostreatus* for 20 min. Scale bars, 25 μm. (****$P < 0.0001$).

and 4-octanone concentrations in which the carbonyl group is on different positions of the carbon chain, for their ability to paralyze *C. elegans*. Both compounds paralyzed *C. elegans* at a similar range of concentrations as observed for 3-octanone (Fig. 8A). Next, we explored whether the length of the carbon chain affects nematode toxicity. We observed that 3-decanone (10 carbons) is more toxic to *C. elegans* than 3-octanone, with concentrations of >30% triggering prominent paralysis. In contrast, 3-hexanone (six carbons) barely elicited nematode paralysis (Fig. 8A), implying that the length of the carbon chain is critical. Next, we examined whether 3-octanone isomers and the small 3-ketones with different carbon chains trigger cell necrosis in ciliated sensory neurons. Apart from 3-hexanone treatment that displayed a limited effect, all other compounds induced obvious fragmentation of neuronal processes after 5 min of treatment (Fig. 8B). Together, these results indicate that the position of the carbonyl group does not regulate biotoxicity, but the length of the carbon chain is critical for nematocidal activity.

DISCUSSION

Eight-carbon VOCs (C_8 VOCs) are prevalent as communication signals in fungi. For example, 1-octen-3-ol, 3-octanone, 3-octanol, 1-octanol, and 2-phenylethanol are conidial germination inhibitors in *Penicillium* and *Aspergillus* (*32*). Similarly, 1-octen-3-ol enhances mycotoxin production in *Penicillium expansum*, whereas 2-phenylethanol inhibits mycotoxin biosynthesis in *Aspergillus flavus* (*33*, *34*). Apart from acting as fungal signals, fungal-derived C_8 VOCs can also regulate plant growth and development. *Trichoderma* emits multiple C_8 VOCs that reduce seed germination and induce a defense response in *Arabidopsis* (*35*, *36*). Moreover, the endophyte *Hypoxylon anthochroum* produces 2-phenylethanol that inhibits seed germination, root elongation, and seedling respiration of plants (*37*). Here, we report that 3-octanone is present in the fragile toxocysts on the hyphae of *P. ostreatus*, and it exerts prominent paralyzing activity on *C. elegans* (Fig. 8C).

Although C_8 VOCs are ubiquitously found in fungi, their bioactive mechanisms remain largely uncharacterized. Previous studies have shown that 1-octen-3-ol exerts mild effects on cell membrane permeability to inhibit spore germination in *Penicillium* and *Aspergillus* (*38*, *39*). Furthermore, C_8 VOCs have been reported to disrupt dopamine packaging and uptake in *Drosophila melanogaster*, causing locomotory defects and dopaminergic neuron degeneration (*40*, *41*). We have shown that 3-octanone disrupts plasma membrane integrity in the neurons, muscle cells, and hypodermis of *C. elegans*, provoking a pronounced calcium influx that, in turn, initiates muscular hypercontraction associated with mitochondrial calcium overload and cell necrosis (Fig. 8C). These phenotypes are reminiscent of the local and systemic skeletal muscle degeneration caused by snakebite envenomation and mass bee attacks, with the phospholipases A_2 in these venoms catalyzing phospholipid hydrolysis or inducing myonecrosis via a nonenzymatic membrane permeabilization mechanism (*2*, *3*). In addition, a variety of bacterial pore-forming toxins—such as Panton-valentine leukocidin from *Staphylococcus aureus* and β-toxin from *Clostridium*

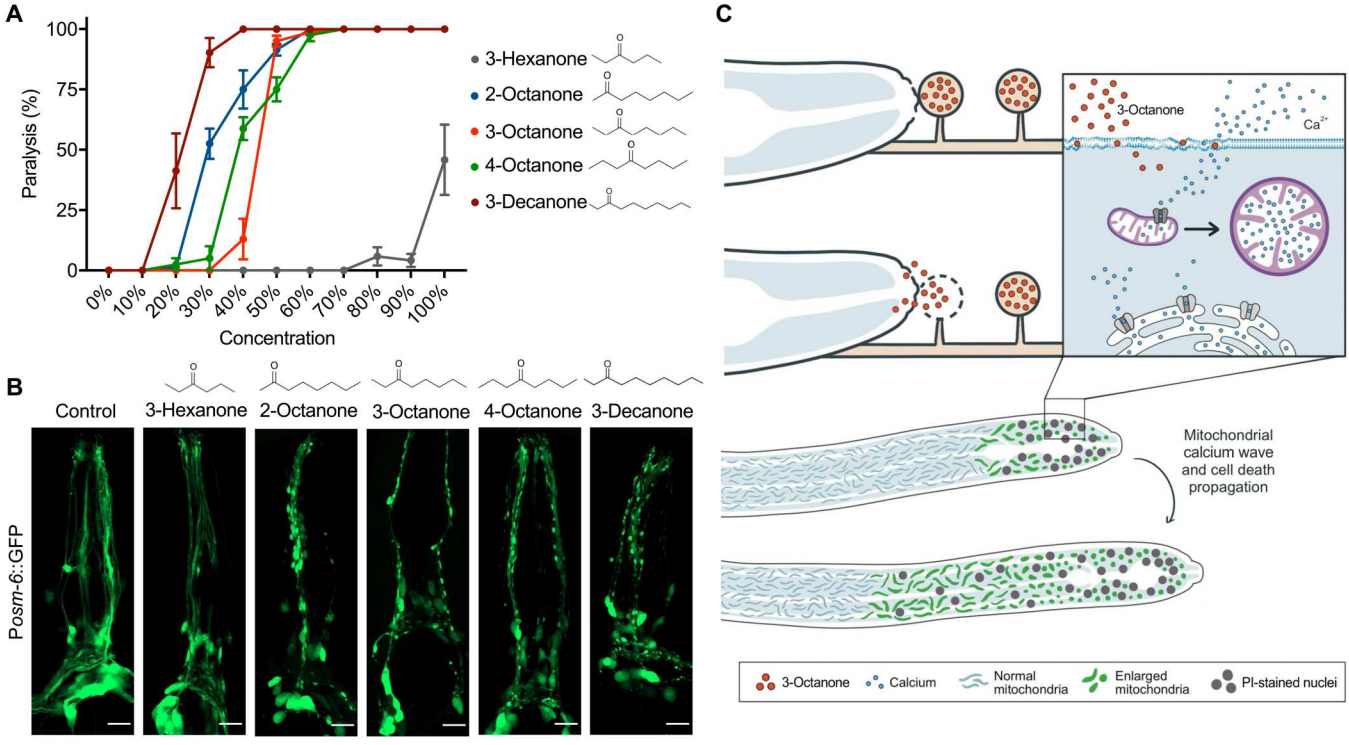

Fig. 8. Compounds structurally related to 3-octanone paralyze *C. elegans*. (**A**) Paralysis ratio of adult N2 upon treatment with 3-octanone or other structurally-related ketones. Each dot represents 20 to 25 animals (means ± SEM; $n = 6$). (**B**) Fluorescence imaging of ciliated sensory neurons using cytosolic GFP reporter lines exposed to 80% 3-octanone or structurally related compounds for 5 min. Scale bars, 10 μm. (**C**) Summary model showing how *P. ostreatus* uses a nerve gas in a lollipop strategy to prey on nematodes. Inset: 3-Octaonone from the toxocysts disrupts plasma membrane integrity, resulting in extracellular calcium influx to the cytosol and mitochondria, which causes mitochondrial swelling.

perfringens—induce necrosis in muscles and intestinal epithelium (*42*–*44*). We have shown that mushrooms, exemplified by *P. ostreatus*, have independently commandeered a naturally occurring C_8 VOC (3-octanone) as a toxin to paralyze nematode prey by compromising plasma membrane integrity in a strategy similar to other venomous organisms.

The dosage of these VOCs is critical to their function. For example, 3-octanone is repellent to slugs and snails at low doses but is lethal at high doses (*45*). We observed that a high concentration (>50%) of 3-octanone is required to recapitulate the fast-acting paralysis, neuronal necrosis, and cell membrane rupture triggered by *P. ostreatus* toxocysts. Moreover, we demonstrate that the cell death propagation and calcium wave induced by toxocysts are dosage dependent, with *C. elegans* individuals that contacted a single toxocyst exhibiting slower and weakened propagation. Given the strong hydrophobic nature of 3-octanone, it is easily solubilized in lipid environments. Therefore, a high concentration of 3-octanone can be readily integrated into lipid bilayers, disrupting lipid organization, as revealed by our in vivo and in vitro liposome experiments (Fig. 5). We propose that the function of toxocysts is to enable 3-octanone accumulation to a sufficiently high local concentration in a system functionally analogous to how the glandular trichomes of plants act as cellular factories for the biosynthesis and storage of large amounts of secondary metabolites providing the first line of defense against herbivores, insects, and pathogens (*5*, *46*). 3-Octanone is also present in the volatiles of many plants (*47*, *48*), indicating that this natural ketone might protect plants from herbivorous insects (*49*). In the future, we plan to investigate the molecular mechanism underlying toxocyst development by first identifying the causative mutations for lost paralytic capability in our suite of *lot* mutants. Last, since 3-octanone alone elicited a slower calcium influx response in the *C. elegans* pharyngeal muscle than triggered by toxocysts, we believe that there might be additional components inside toxocysts that might function synergistically with 3-octanone.

Why has the genus *Pleurotus* evolved these toxocyst structures that accumulate 3-octanone to kill nematodes? *Pleurotus* are white-rot fungi that mostly live on dying/rotting hardwood trees where nitrogen is extremely limited (*50*). One possible explanation for their predatory activity on nematodes is to acquire nutrients to survive in these nitrogen-poor environments. Furthermore, *Pleurotus* shares the same ecological niche as some genera of frugivorous nematodes, such as *Bursaphelenchus* and *Paraphelenchus*. These frugivorous nematodes can pierce fungal hyphae with their strong stylet to suck out the cytoplasm (*51*, *52*). Thus, toxocysts might also serve as a defensive structure against nematode predators. Future studies that explore how toxocyst development is regulated by environmental or physiological factors might reveal strategies for developing *P. ostreatus* as an effective biocontrol agent against parasitic nematodes in agriculture. In summary, our work has revealed that the carnivorous mushroom *P. ostreatus* has evolved a "nerve gas in a lollipop" strategy to rapidly paralyze and kill nematodes. Toxocysts enable the accumulation of a volatile ketone, 3-octanone, to a high local concentration that disrupts cell membrane integrity and causes rapid cell and organismal death in nematodes.

MATERIALS AND METHODS

Nematode and fungal strains

Nematodes were grown on nematode growth medium (NGM) agar plates seeded with OP50 bacteria at room temperature. Mutant strains were obtained from the Caenorhabditis Genetics Center or were generated using a CRISPR-Cas9 approach (*53*). Transgenic animals were generated using standard microinjection techniques (*54*). *P. ostreatus* strain PC9 was used in this study (*55*–*57*). Fungal cultures were maintained on potato dextrose agar (Difco), yeast extract, malt extract, and glucose (YMG), or low-nutrient mineral salt (LNM) (2% agar, 1.66 mM $MgSO_4$, 5.4 μM $ZnSO_4$, 2.6 μM $MnSO_4$, 18.5 μM $FeCl_3$, 13.4 mM KCl, 0.34 μM biotin, and 0.75 μM thiamin) medium. The nematode and fungal strains used in this study are listed in table 2.

Mutagenesis and forward genetic screening

Protoplasts of *P. ostreatus* were generated following a standard protocol (*58*, *59*). The protoplasts were treated with EMS (6 μg/ml) or treated for 3 or 6 s with 15 W of UV. Grown colonies were picked onto 48-well YMG plates and then transferred to 48-well LNM plates. To screen for the paralyzing ability of mutants, *P. ostreatus* colonies were cultured on 48-well LNM plates for 5 days before adding ~40 *C. elegans* into each well. After 24 hours, mutants defective in paralyzing nematodes were selected for rescreening.

C. elegans paralysis assay

To quantify the paralysis ratio of nematodes in response to *P. ostreatus*, 15 adult N2-strain *C. elegans* were transferred to fungal cultures for 5 min, before assessing paralysis phenotypes such as head muscle hypercontraction, cessation of pharyngeal pumping, and impaired locomotion. To test the bioactivity of 3-octanone and its structurally related compounds in terms of paralyzing nematodes, various concentrations of the compounds were added directly on nematodes to reflect direct contact. Paralysis phenotypes were assessed after 30 min.

Calcium imaging

To monitor cytosolic or mitochondrial calcium levels in pharyngeal muscle cells, animals carrying yphIs3(P*myo-2*::GCaMP6s) and yphIs13(P*myo-2*::MTS::GCaMP5) were exposed to *P. ostreatus*, *lot* mutants, 1 μl of 50% 3-octanone, or the solvent control, and then calcium responses were recorded using a Zeiss SteREO V20 microscope with an Andor Zyla 5.5 sCMOS camera. MetaXpress with a customized module was used to calculate the fluorescence intensity of GCaMP in the pharyngeal corpus as the region of interest (ROI). F represents the signal intensity of the ROI-subtracted background fluorescence. F_0 is the average F of the first 10 to 20 s of each video. To monitor the mitochondrial calcium response in the hypodermis, animals that carried yphIs17(P*col-19*::MTS::GCaMP5) were exposed to *P. ostreatus* culture for the desired time intervals, and the calcium level was analyzed via an Andor Revolution WD system with a Nikon Ti-E automatic microscope and an XON Ultra 888 EMCCD camera (Andor). The extent of fluorescence was determined according to activated GCaMP signals in an anterior-to-posterior direction and quantified in MetaMorph.

Fluorescence imaging

To image the morphology of cells, mitochondria, and plasma membranes in various cell types, nematodes hosting the yphEx301(P*osm-6*::MTS::roGFP), yphEx302(P*myo-2*::MTS::roGFP), zcIs14(P*myo-3*::MTS::GFP), yphIs17(P*col-19*::MTS::GCaMP5), yphEx306(P*myo-3*::myrGFP), yphEx307(P*klp-6*::myrGFP), yphEx309(P*col-19*::memGFP), and yphEx216(P*osm-6*::GFP) plasmids were used. Animals were exposed to *P. ostreatus* or 1 μl of 80% 3-octanone for 5 or 10 min, then placed on 3% agar pads on glass slides with 2 μl of 500 mM NaN_3, and imaged using an LSM 980 Airyscan 2 confocal microscope (Carl Zeiss) with a C-Apochromat 63×/1.2 numerical aperture (NA) water immersion objective. Images were acquired with Multiplex Mode (SR-4Y) and analyzed in Zeiss ZEN blue software.

PI staining and ATP measurement

To determine membrane integrity, adult nematodes were exposed to *P. ostreatus* or 1 μl of 80% 3-octanone for 1 min, subjected to 5 μl of PI solution (final concentration, 0.1 mM; P3566, Invitrogen), and imaged using an Andor Revolution WD camera with a Nikon Ti-E automatic microscope. To measure ATP levels in pharyngeal muscle and hypodermis, animals carrying yphEx304(P*myo-2*::QUEEN-2m) or yphEx305(P*col-19*::QUEEN-2m) were exposed to *P. ostreatus* or 1 μl of 50% 3-octanone and analyzed by the same device described above with an Apo LWD 40×/1.15 NA water immersion objective. Images were captured with an iXon Ultra 888 EMCCD camera (Andor) and analyzed with MetaMorph. QUEEN-2m was excited by 488- and 405-nm lasers (*26*), and the 405/488 excitation ratio was analyzed in ImageJ.

Imaging of fungal morphology

P. ostreatus was cultured on LNM medium for 14 days at 25°C. Fungal hyphae were imaged using a Zeiss SteREO V20 microscope with an Andor Zyla 5.5 sCMOS camera. To image the ultrastructure of *Pleurotus* toxocysts, we performed scanning electron microscopy (SEM). Fungal cultures were cryofixed with liquid nitrogen and sputter-coated with a 3- to 5-nm platinum (Pt) coating at −130°C. Images were acquired via an FEI Quanta 200 SEM with a cryo system (Quorum PP2000TR FEI) at 20 kV.

Transmission electron microscopy

One-day-old adult nematodes were exposed to *P. ostreatus* or 1 μl of 80% 3-octanone for 5 min and placed into an *E. coli*–filled planchette. Samples were immediately loaded into a freezing holder and frozen in a high-pressure freezing machine (Leica HPM 100) for cryofixation. Frozen samples in planchettes were transferred to a liquid nitrogen bath containing the freeze-substitution solution. Next, samples were transferred to a Spurr′s resin/acetone (1:9) solution and gradually infiltrated with resin. Ultrathin sections (75 nm) were poststained with 1% aqueous uranyl acetate and Reynolds′ lead citrate solution, and then images were acquired using a Thermo Fisher Scientific Talos L120C transmission electron microscope at 120 kV equipped with a 4000 × 4000 Ceta CMOS camera.

N2 liposome morphology was also investigated by TEM (Tecnai G2 Spirit TWIN, Thermo Fisher Scientific). Volumes of 4 μl of liposome solution [N2 lipids (2 mg/ml) in 20 mM tris-HCl buffer (pH 7.5)] were treated with a 0, 50, or 80% final concentration of 3-octanone for 5 min. Negative staining was performed as described previously (*60*). Samples were transferred to glow-discharged grids for 30 s and then stained with 1% uranyl acetate for 30 s. Electron micrographs were recorded at a nominal magnification of ×11,000 at 80 kV using a 3000 × 4000 GATAN CCD SC1000 camera.

GC-MS analysis

Profiling of *P. ostreatus* volatiles was conducted using a solid-phase microextraction method coupled with a GC-MS system. First, *P. ostreatus* was cultured in a 20-ml glass vial tightly capped with a polytetrafluoroethylene/silicone magnetic headspace cap. To extract volatile compounds from the samples, as well as a medium control, a carboxen/polydimethylsiloxane fiber was used and preconditioned at 300°C for 5 min. The fiber was inserted into the sample vial through the septum and exposed to the headspace at 25°C for 90 min to extract the analytes. Next, the fiber was removed from the vial and inserted into the injection port of the GC-MS system to analyze volatile compounds. The injection temperature was set at 250°C, and the injection type was operated in splitless mode. The volatile compounds were analyzed using an Agilent 7890B gas chromatography system coupled with a 7250 quadrupole time-of-flight mass spectrometer equipped with electron ionization (EI). Separation was performed via a Zorbax DB5-MS + 10-m Duragard Capillary Column (30 m by 0.25 mm by 0.25 mm; Agilent). The GC temperature profile was held at 40°C for 1 min, then raised by 10°C/min to 300°C, and lastly held at 300°C for 3 min. The transfer line and the ion source temperature were set at 300° and 280°C, respectively. The mass range was monitored from 50 to 600 Da. Mass spectra were compared against the NIST 2017 and Wiley Registry 11th Edition mass spectral libraries.

Hydroxylamine HCl analysis

P. ostreatus wild-type and *lot* mutants were cultured on a 9-cm LNM plate for 15 days. *P. ostreatus* fungal culture was mixed with 1 mM hydroxylamine solution. The salt and remaining impurities from the sample were removed by solid-phase extraction using an Oasis HLB cartridge (Waters, USA). The cartridge was first conditioned with 600 μl of 100% acetonitrile and equilibrated with 600 μl of 50% acetonitrile in 0.1% formic acid aqueous solution, followed by 600 μl of double-distilled H_2O (ddH_2O). The sample (400 μl) was loaded and desalted twice with 400 μl of ddH_2O. The eluent was collected by adding 400 μl of 50% acetonitrile in 0.1% formic acid aqueous solution to the same Eppendorf tube. Then, the final sample was detected by in situ nanospray ionization in a mass spectrometer equipped with a quadrupole mass filter/time-of-flight system (High Definition Mass Spectrometry, HDMS; Waters, UK) operated in electrospray-positive mode.

Preparation of liposomes using total lipid extracts from *C. elegans*

Total lipid extraction of *C. elegans* was carried out via the Bligh′s extraction approach (*61*). The dried lipid extracts were resuspended in 20 mM tris-HCl (pH 7.5), with a stock concentration of 10 mg/ml (w/v). The liposomes were then prepared by extrusion using an Avanti Mini-Extruder (Avanti Polar Lipids, catalog no. 610000), and the diameter of liposomes was controlled using a Nuclepore Track-Etch Membrane with a 0.1-μm pore size (Whatman, catalog no. 800309) (*62*).

Turbidity measurement of liposomes

To measure the turbidity of liposomes, liposomes (2 mg/ml) from extracted *C. elegans* N2 lipids in 20 mM tris-HCl (pH 7.5) was mixed with 3-octanone. The final concentrations of 3-octanone were 0, 50, or 80% (v/v). The absorbance of each liposome and 3-octanone mixture at 400 nm was measured using an EnSpire Multimode Plate Reader (PerkinElmer) for a total of 12 min at 25°C. During the measurement, solutions were remixed every 2.5 min to maintain their homogeneity.

Statistics

An unpaired two-tailed Student's *t* test was performed to determine the statistical difference between control and experimental samples in GraphPad Prism 9. $P < 0.05$ was considered significant; asterisks demonstrate statistical significance, as calculated by Student's *t* test ($^{*}P < 0.05$, $^{**}P < 0.01$, $^{***}P < 0.001$, and $^{****}P < 0.0001$).

Supplementary Materials

This PDF file includes:
Figs. S1 to S6

Other Supplementary Material for this manuscript includes the following:
Movies S1 to S7

REFERENCES AND NOTES

1. T. C. Südhof, α-Latrotoxin and its receptors: Neurexins and CIRL/latrophilins. *Annu. Rev. Neurosci.* **24**, 933–962 (2001).
2. A. L. Oliveira, M. F. Viegas, S. L. da Silva, A. M. Soares, M. J. Ramos, P. A. Fernandes, The chemistry of snake venom and its medicinal potential. *Nat. Rev. Chem.* **6**, 451–469 (2022).
3. C. Montecucco, J. M. Gutiérrez, B. Lomonte, Cellular pathology induced by snake venom phospholipase A_2 myotoxins and neurotoxins: Common aspects of their mechanisms of action. *Cell. Mol. Life Sci.* **65**, 2897–2912 (2008).
4. A. Huchelmann, M. Boutry, C. Hachez, Plant glandular trichomes: Natural cell factories of high biotechnological interest. *Plant Physiol.* **175**, 6–22 (2017).
5. G. J. Wagner, Secreting glandular trichomes: More than just hairs. *Plant Physiol.* **96**, 675–679 (1991).
6. R. J. Harris, R. A. Jenner, Evolutionary ecology of fish venom: Adaptations and consequences of evolving a venom system. *Toxins (Basel)* **11**, 60 (2019).
7. G. L. Barron, *The Nematode-Destroying Fungi* (Canadian Biological Publications Ltd., 1977).
8. B. Nordbring-Hertz, Nematophagous fungi: Strategies for nematode exploitation and for survival. *Microbiol. Sci.* **5**, 108–116 (1988).
9. J. Van Den Hoogen, S. Geisen, D. Routh, H. Ferris, W. Traunspurger, D. A. Wardle, R. G. M. de Goede, B. J. Adams, W. Ahmad, W. S. Andriuzzi, R. D. Bardgett, M. Bonkowski, R. Campos-Herrera, J. E. Cares, T. Caruso, L. de Brito Caixeta, X. Chen, S. R. Costa, R. Creamer, J. M. da Cunha Castro, M. Dam, D. Djigal, M. Escuer, B. S. Griffiths, C. Gutiérrez, K. Hohberg, D. Kalinkina, P. Kardol, A. Kergunteuil, G. Korthals, V. Krashevska, A. A. Kudrin, Q. Li, W. Liang, M. Magilton, M. Marais, J. A. R. Martín, E. Matveeva, E. H. Mayad, C. Mulder, P. Mullin, R. Neilson, T. A. D. Nguyen, U. N. Nielsen, H. Okada, J. E. P. Rius, K. Pan, V. Peneva, L. Pellissier, J. C. P. da Silva, C. Pitteloud, T. O. Powers, K. Powers, C. W. Quist, S. Rasmann, S. S. Moreno, S. Scheu, H. Setälä, A. Sushchuk, A. V. Tiunov, J. Trap, W. van der Putten, M. Vestergård, C. Villenave, L. Waeyenberge, D. H. Wall, R. Wilschut, D. G. Wright, J.-I. Yang, T. W. Crowther, Soil nematode abundance and functional group composition at a global scale. *Nature* **572**, 194–198 (2019).
10. D. Pramer, Nematode-trapping fungi: An intriguing group of carnivorous plants inhabit the microbial world. *Science* **144**, 382–388 (1964).
11. Y.-P. Hsueh, M. R. Gronquist, E. M. Schwarz, R. D. Nath, C. H. Lee, S. Gharib, F. C. Schroeder, P. W. Sternberg, Nematophagous fungus *Arthrobotrys oligospora* mimics olfactory cues of sex and food to lure its nematode prey. *eLife* **6**, e20023 (2017).
12. Y.-P. Hsueh, P. Mahanti, F. C. Schroeder, P. W. Sternberg, Nematode-trapping fungi eavesdrop on nematode pheromones. *Curr. Biol.* **23**, 83–86 (2013).
13. Y. Yang, E. Yang, Z. An, X. Liu, Evolution of nematode-trapping cells of predatory fungi of the Orbiliaceae based on evidence from rRNA-encoding DNA and multiprotein sequences. *Proc. Natl. Acad. Sci. U.S.A.* **104**, 8379–8384 (2007).
14. G. L. Barron, R. G. Thorn, Destruction of nematodes by species *of Pleurotus*. *Can. J. Bot.* **65**, 774–778 (1987).
15. C.-H. Lee, H.-W. Chang, C.-T. Yang, N. Wali, J.-J. Shie, Y.-P. Hsueh, Sensory cilia as the Achilles heel of nematodes when attacked by carnivorous mushrooms. *Proc. Natl. Acad. Sci. U.S.A.* **117**, 6014–6022 (2020).
16. O. C. H. Kwok, R. Plattner, D. Weisleder, D. T. Wicklow, A nematicidal toxin from *Pleurotus ostreatus* NRRL 3526. *J. Chem. Ecol.* **18**, 127–136 (1992).
17. R. W. Burg, B. M. Miller, E. E. Baker, J. Birnbaum, S. A. Currie, R. Hartman, Y.-L. Kong, R. L. Monaghan, G. Olson, I. Putter, J. B. Tunac, H. Wallick, E. O. Stapley, R. Oiwa, S. Ōmura, Avermectins, new family of potent anthelmintic agents: Producing organism and fermentation. *Antimicrob. Agents Chemother.* **15**, 361–367 (1979).
18. J. A. Dent, M. M. Smith, D. K. Vassilatis, L. Avery, The genetics of ivermectin resistance in *Caenorhabditis elegans*. *Proc. Natl. Acad. Sci. U.S.A.* **97**, 2674–2679 (2000).
19. J. A. Dent, M. W. Davis, L. Avery, avr-15 encodes a chloride channel subunit that mediates inhibitory glutamatergic neurotransmission and ivermectin sensitivity in *Caenorhabditis elegans*. *EMBO J.* **16**, 5867–5879 (1997).
20. F. Zhang, D. Peng, C. Cheng, W. Zhou, S. Ju, D. Wan, Z. Yu, J. Shi, Y. Deng, F. Wang, X. Ye, Z. Hu, J. Lin, L. Ruan, M. Sun, *Bacillus thuringiensis* crystal protein Cry6Aa triggers *Caenorhabditis elegans* necrosis pathway mediated by aspartic protease (ASP-1). *PLOS Pathog.* **12**, e1005389 (2016).
21. J. S. Griffitts, J. L. Whitacre, D. E. Stevens, R. V. Aroian, Bt toxin resistance from loss of a putative carbohydrate-modifying enzyme. *Science* **293**, 860–864 (2001).
22. B.-N. Truong, A. Suzuki, B.-N. Truong, K. Okazaki, T. Fukiharu, Y. Takeuchi, K. Futai, X.-T. Le, A. Suzuki, Characterization of the nematocidal toxocyst in *Pleurotus* subgen. *Coremiopleurotus*. *Mycoscience* **48**, 222–230 (2007).
23. I. Szabo, M. Zoratti, Mitochondrial channels: Ion fluxes and more. *Physiol. Rev.* **94**, 519–608 (2014).
24. R. Viveiros, H. Hutter, D. G. Moerman, Membrane extensions are associated with proper anterior migration of muscle cells during *Caenorhabditis elegans* embryogenesis. *Dev. Biol.* **358**, 189–200 (2011).
25. Y. Tsujimoto, Apoptosis and necrosis: Intracellular ATP level as a determinant for cell death modes. *Cell Death Differ.* **4**, 429–434 (1997).
26. H. Yaginuma, S. Kawai, K. V. Tabata, K. Tomiyama, A. Kakizuka, T. Komatsuzaki, H. Noji, H. Imamura, Diversity in ATP concentrations in a single bacterial cell population revealed by quantitative single-cell imaging. *Sci. Rep.* **4**, 6522 (2014).
27. R. Bodhicharla, R. Devkota, M. Ruiz, M. Pilon, Membrane fluidity is regulated cell nonautonomously by *Caenorhabditis elegans* PAQR-2 and its mammalian homolog AdipoR2. *Genetics* **210**, 189–201 (2018).
28. E. Svensk, M. Ståhlman, C.-H. Andersson, M. Johansson, J. Borén, M. Pilon, PAQR-2 regulates fatty acid desaturation during cold adaptation in *C. elegans*. *PLOS Genet.* **9**, e1003801 (2013).
29. E. Svensk, R. Devkota, M. Ståhlman, P. Ranji, M. Rauthan, F. Magnusson, S. Hammarsten, M. Johansson, J. Borén, M. Pilon, *Caenorhabditis elegans* PAQR-2 and IGLR-2 protect against glucose toxicity by modulating membrane lipid composition. *PLOS Genet.* **12**, e1005982 (2016).
30. H. Ahyayauch, M. Bennouna, A. Alonso, F. M. Goñi, Detergent effects on membranes at subsolubilizing concentrations: Transmembrane lipid motion, bilayer permeabilization, and vesicle lysis/reassembly are independent phenomena. *Langmuir* **26**, 7307–7313 (2010).
31. J. R. Henriksen, T. L. Andresen, L. N. Feldborg, L. Duelund, J. H. Ipsen, Understanding detergent effects on lipid membranes: A model study of lysolipids. *Biophys. J.* **98**, 2199–2205 (2010).
32. K. K. Pennerman, G. Yin, J. W. Bennett, Eight-carbon volatiles: Prominent fungal and plant interaction compounds. *J. Exp. Bot.* **73**, 487–497 (2022).
33. S. S. T. Hua, J. J. Beck, S. B. L. Sarreal, W. Gee, The major volatile compound 2-phenylethanol from the biocontrol yeast, *Pichia anomala*, inhibits growth and expression of aflatoxin biosynthetic genes of *Aspergillus flavus*. *Mycotoxin Res.* **30**, 71–78 (2014).
34. K. K. Pennerman, J. B. Scarsella, G.-H. Yin, S.-S. T. Hua, T. G. Hartman, J. W. Bennett, Volatile 1-octen-3-ol increases patulin production by *Penicillium expansum* on a patulin-suppressing medium. *Mycotoxin Res.* **35**, 329–340 (2019).
35. K. Kishimoto, K. Matsui, R. Ozawa, J. Takabayashi, Volatile 1-octen-3-ol induces a defensive response in *Arabidopsis thaliana*. *J. Gen. Plant Pathol.* **73**, 35–37 (2007).
36. R. Hung, S. Lee, C. Rodriguez-Saona, J. W. Bennett, Common gas phase molecules from fungi affect seed germination and plant health in *Arabidopsis thaliana*. *AMB Express* **4**, 53 (2014).

37. Á. Ulloa-Benítez, Y. M. Medina-Romero, R. E. Sánchez-Fernández, P. Lappe-Oliveras, G. Roque-Flores, G. Duarte Lisci, T. Herrera Suárez, M. L. Macías-Rubalcava, Phytotoxic and antimicrobial activity of volatile and semi-volatile organic compounds from the endophyte *Hypoxylon anthochroum* strain Blaci isolated from Bursera lancifolia (Burseraceae). *J. Appl. Microbiol.* **121**, 380–400 (2016).
38. G. Yin, S. Padhi, S. Lee, R. Hung, G. Zhao, J. W. Bennett, Effects of three volatile oxylipins on colony development in two species of fungi and on *Drosophila* larval metamorphosis. *Curr. Microbiol.* **71**, 347–356 (2015).
39. G. S. Chitarra, T. Abee, F. M. Rombouts, J. Dijksterhuis, 1-Octen-3-ol inhibits conidia germination of *Penicillium paneum* despite of mild effects on membrane permeability, respiration, intracellular pH, and changes the protein composition. *FEMS Microbiol. Ecol.* **54**, 67–75 (2005).
40. A. A. Inamdar, M. M. Hossain, A. I. Bernstein, G. W. Miller, J. R. Richardson, J. W. Bennett, Fungal-derived semiochemical 1-octen-3-ol disrupts dopamine packaging and causes neurodegeneration. *Proc. Natl. Acad. Sci.* **110**, 19561–19566 (2013).
41. A. A. Inamdar, P. Masurekar, J. W. Bennett, Neurotoxicity of fungal volatile organic compounds in *Drosophila melanogaster*. *Toxicol. Sci.* **117**, 418–426 (2010).
42. V. Finck-Barbançon, G. Duportail, O. Meunier, D. A. Colin, Pore formation by a two-component leukocidin from *Staphyloccocus aureus* within the membrane of human polymorphonuclear leukocytes. *Biochimica et Biophysica Acta* **1182**, 275–282 (1993).
43. V. Steinthorsdottir, H. Halldórsson, O. S. Andrésson, *Clostridium perfringens* beta-toxin forms multimeric transmembrane pores in human endothelial cells. *Microb. Pathog.* **28**, 45–50 (2000).
44. F. C. Los, T. M. Randis, R. V. Aroian, A. J. Ratner, Role of pore-forming toxins in bacterial infectious diseases. *Microbiol. Mol. Biol. Rev.* **77**, 173–207 (2013).
45. S. Khoja, K. M. Eltayef, I. Baxter, J. C. Bull, E. J. Loveridge, T. Butt, Fungal volatile organic compounds show promise as potent molluscicides. *Pest Manag. Sci.* **75**, 3392–3404 (2019).
46. Z. Feng, E. S. Bartholomew, Z. Liu, Y. Cui, Y. Dong, S. Li, H. Wu, H. Ren, X. Liu, Glandular trichomes: New focus on horticultural crops. *Horticulture Res.* **8**, 158 (2021).
47. A. Koedam, M. J. M. Gijbels, Isolation and identification of 3-octanone in the essential oil of *Rosmarinus officinalis* L. *Z. Naturforsch. C* **33**, 144–145 (1978).
48. G. R. Takeoka, R. A. Flath, M. Guentert, W. Jennings, Nectarine volatiles: Vacuum steam distillation versus headspace sampling. *J. Agric. Food Chem.* **36**, 553–560 (1988).
49. P.-A. Bourdon, M. Zottele, I. Baxter, A. Myrta, A. Midthassel, K. F. Wechselberger, S. Khoja, J. C. Bull, S. Hermann, T. M. Butt, Fumigation of three major soil pests (*Agriotes lineatus, Diabrotica virgifera virgifera, Phyllopertha horticola*) with 3-octanone and 1-octen-3-ol enantiomers. *Biocontrol Sci. Technol.* **32**, 863–876 (2022).
50. R. Cohen, L. Persky, Y. Hadar, Biotechnological applications and potential of wood-degrading mushrooms of the genus Pleurotus. *Appl. Microbiol. Biotechnol.* **58**, 582–594 (2002).
51. K. Futai, Pine wood nematode, Bursaphelenchus xylophilus. *Annu. Rev. Phytopathol.* **51**, 61–83 (2013).
52. G. W. Yeates, T. Bongers, R. G. De Goede, D. W. Freckman, S. Georgieva, Feeding habits in soil nematode families and genera—An outline for soil ecologists. *J. Nematol.* **25**, 315–331 (1993).
53. H. Wang, H. Park, J. Liu, P. W. Sternberg, An efficient genome editing strategy to generate putative null mutants in *Caenorhabditis elegans* using CRISPR/Cas9. *G3* **8**, 3607–3616 (2018).
54. C. C. Mello, J. M. Kramer, D. Stinchcomb, V. Ambros, Efficient gene transfer in *C. elegans*: Extrachromosomal maintenance and integration of transforming sequences. *EMBO J.* **10**, 3959–3970 (1991).
55. L. Larraya, M. M. Peñas, G. Pérez, C. Santos, E. Ritter, A. G. Pisabarro, L. Ramírez, Identification of incompatibility alleles and characterisation of molecular markers genetically linked to the *a* incompatibility locus in the white rot fungus *Pleurotus ostreatus*. *Curr. Genet.* **34**, 486–493 (1999).
56. L. M. Larraya, G. Pérez, M′. M. Peñas, J. J. P. Baars, T. S. P. Mikosch, A. G. Pisabarro, L′. Ramírez, Molecular karyotype of the white rot fungus *Pleurotus ostreatus*. *Appl. Environ. Microbiol.* **65**, 3413–3417 (1999).
57. Y.-Y. Lee, G. Vidal-Diez de Ulzurrun, E. M. Schwarz, J. E. Stajich, Y.-P. Hsueh, Genome sequence of the oyster mushroom *Pleurotus ostreatus* strain PC9. *G3* **11**, jkaa008 (2021).
58. Y. Honda, T. Matsuyama, T. Irie, T. Watanabe, M. Kuwahara, Carboxin resistance transformation of the homobasidiomycete fungus *Pleurotus ostreatus*. *Curr. Genet.* **37**, 209–212 (2000).
59. T. Irie, Y. Honda, T. Watanabe, M. Kuwahara, Efficient transformation of filamentous fungus *Pleurotus ostreatus* using single-strand carrier DNA. *Appl. Microbiol. Biotechnol.* **55**, 563–565 (2001).
60. U. Baxa, in *Characterization of Nanoparticles Intended for Drug Delivery*, S. E. McNeil, Ed. (Springer New York, 2018), pp. 73–88.
61. E. G. Bligh, W. J. Dyer, A fast total lipid extraction and purification method. *Can. J. Biochem. Physiol.* **37**, 911–917 (1959).
62. O. H. Voss, H.-N. Lee, L. Tian, K. Krzewski, J. E. Coligan, Liposome preparation for the analysis of lipid-receptor interaction and efferocytosis. *Curr. Protoc. Immunol.* **120**, 14.44.11–14.44.21 (2018).

Acknowledgments: We thank the Caenorhabditis Genetics Center (CGC), WormBase, P. W. Sternberg, and C.-L. Pan for sharing the nematode strains and U. Kües and Y. Hadar for helpful suggestions on growing *P. ostreatus* and sharing the fungal strains. We thank C.-Y. Lin and C.-Y. Ting at the Metabolomics Core Facility, Agricultural Biotechnology Research Center at Academia Sinica for assisting with solid-phase microextraction method coupled with a GC-MS parameter optimization and data analysis. We thank W.-N. Jane and Y.-C. Chou at the Electron Microscope Division, Cell Biology Core Lab in IPMB, Academia Sinica for assisting with SEM operation. We are grateful to H.-M. Li, C.-L. Pan, and M.-C. Yao for comments and suggestions on the manuscript and L.-M. Hsu and A.-M. Yang for the technical assistance in the laboratory. We thank S.-C. Juan for designing the graphic model and J. O'Brien for editing the manuscript. **Funding:** This work was supported by the Academia Sinica Career Development Award AS-CDA-106-L03, Investigator Award AS-IA-111-L02 and the MOST grant 110-2311-B-001-047-MY3 to Y.-P.H. We also thank EMBO Global Investigator Network and Young Investigator Program for supports to Y.-P.H. The CGC is funded by the NIH Office of Research Infrastructure Programs (P40 OD010440). **Author contributions:** C.-H.L., Y.-Y.L., and Y.-P.H. designed the research. C.-H.L., Y.-Y.L., Y.-C.C., W.-L.P., S.-P.L., and J.-J.S. performed the research. C.-H.L., Y.-Y.L., Y.-C.C., N.W., T.N., Y.H., and J.-J.S. contributed new reagents/analytical tools. C.-H.L., Y.-Y.L., Y.-C.C., N.W., J.-J.S., and Y.-P.H. analyzed the data. C.-H.L. and Y.-P.H. wrote the paper. **Competing interests:** The authors declare that they have no competing interests. **Data and materials availability:** All data needed to evaluate the conclusions in the paper are present in the paper and/or the Supplementary Materials.

Submitted 18 August 2022
Accepted 16 December 2022
Published 18 January 2023
10.1126/sciadv.ade4809